Polymer Chemistry

ROYAL SOCIETY OF CHEMISTRY

PAPER

View Article Online
View Journal | View Issue

Cite this: *Polym. Chem.*, 2024, **15**, 1212

Phosphorus acid: an asset for flame-retardant sustainable vitrimers†

Florian Cuminet,[a,b] Nathan Vanachte,[a] Chloé Farina,[a] Maxinne Denis,[a] Claire Negrell,[a] Sylvain Caillol,*[a] Éric Dantras,[b] Éric Leclerc[a] and Vincent Ladmiral*[a]

Received 2nd December 2023,
Accepted 16th February 2024

DOI: 10.1039/d3py01328f

rsc.li/polymers

Three biobased epoxy resins from vanillic alcohol, linseed oil and cardanol were crosslinked with phosphoric acid to prepare vitrimers. The reactivities of the different types of epoxy towards phosphoric acid were assessed by ^{1}H and ^{31}P NMR spectroscopy on model molecules. The resulting phosphate esters constitute the nodes of the network, which can exchange with free hydroxy groups upon heating, thus conferring reshaping capability to the materials. Additionally, the phosphate groups endow flame retardant properties to the materials. When exposed to fire a char layer is formed, which insulates the inner part of the material and slows down its combustion. Finally, mixtures of the three epoxy resins led to dynamic materials with both fire retardancy properties and low T_g.

Introduction

Vitrimers are polymeric materials at the crossroads of thermosets and thermoplastics, able to be mechanically reprocessed and endowed with high chemical resistance.[1] They are made of a tridimensional macromolecular network whose covalent bonds are dynamic thanks to bond or functional group exchanges.[2] This peculiar property makes them able to flow and change shape upon heating.

Since the first vitrimer, based on catalyzed transesterification,[3] several strategies have been developed to obtain fast exchanges in such materials. Indeed, sufficiently fast exchange at moderately high temperature is desirable to attain acceptable reprocessing times and avoid degradation. In particular, numerous different exchange reactions were investigated[4,5] such as vinylogous urethane transamination,[6] imine metathesis[7] or olefins metathesis[8] to name a few. Alternatively, the rate of a slow exchange reaction can be enhanced by the use of catalysts. This approach is typical for transesterification vitrimers for instance.[3,5] Another strategy consists in exploiting well-chosen and judiciously located activating groups in the network to accelerate the exchange reaction.[9–14] Surprisingly, in this quest for fast exchanges, limited interest was given to phosphate esters despite their known easy exchange with alcohols.[15] Phosphates were used as adhesion promoters in polyimine vitrimers.[16] The transesterification of carboxylate esters in vitrimers was also catalyzed by phosphates and phosphonates.[17–22] Nonetheless, few articles reported the use of phosphate esters as the exchange sites in vitrimers. Exchanges can happen between phosphate esters and carboxylate esters,[23] and even *via* a dissociative pathway involving a cyclization to make a dynamic network.[24] However, the associative exchange of a phosphate ester with a hydroxyl moiety is the most common. For example, a vitrimer was prepared by anionic polymerization of bisphenol A diglycidyl ether (BADGE) in ionic liquid containing phosphates. The resulting phosphate esters were the crosslinking nodes of the network.[25] Feng and Li also reported vitrimers based on BADGE crosslinked by phosphate diesters.[26,27] The dynamic behaviour of phosphate ester based vitrimers was much faster compared to their carboxylic ester counterparts. The exchange can even be accelerated by hydroxyl groups in close vicinity to phosphate ester bonds.[28] Furthermore, phosphates added fire retardancy properties to the materials.[29] Another article reported epoxidized rubber crosslinked by D-fructose 1,6-bisphosphoric acid as an example of biobased vitrimer elastomer.[30] Phytic acid, a naturally occurring polyphosphoric acid, was used to crosslink epoxidized itaconic acid to obtain fully biobased fire retardant vitrimers.[31] Finally, Sijbesma *et al.* described a network with phosphate triesters as crosslinking nodes.[32] The material was a vitrimer, resulting from the reaction between a polyol and triphenyl phosphate in the presence of sodium hydride. The phosphate ester vitrimers described so far were based on difunctional phosphoric acid monoesters. However, the use of phosphoric acid H_3PO_4 has not been reported yet in such

[a]ICGM, Univ Montpellier, CNRS, ENSCM, Montpellier, France.
E-mail: sylvain.caillol@enscm.fr, vincent.ladmiral@enscm.fr
[b]CIRIMAT, Université Toulouse 3 – Paul Sabatier, Physique des Polymères, 118 Route de Narbonne, 31062 Toulouse, France

†Electronic supplementary information (ESI) available. See DOI: https://doi.org/10.1039/d3py01328f

materials. Phosphoric acid bears three acid functions able to react with epoxides to produce beta-hydroxyl phosphoester functional groups susceptible to fast transesterification.

In this work, the reactivities of different epoxy functions towards phosphoric acid were assessed *via* ^{1}H NMR spectroscopy studies on model molecules. Then, three biobased epoxy resins with different structures were polymerized with phosphoric acid H_3PO_4 and the thermal and mechanical behaviors of the materials obtained were compared, in particular their dynamic and flame-retardant properties. Binary and ternary mixtures of the epoxy monomers could also be used to tune the properties of the final materials.

Results and discussion

Epoxy resins

Diglycidyl ether of vanillic alcohol (DGEVA) is derived from vanillin,[33] a compound found in vanilla which can be produced industrially from lignocellulosic materials.[34] Vanillin is first reduced to vanillic alcohol prior to glycidylation by epichlorohydrin, which can be biobased,[35] to finally reach DGEVA (Scheme 1). DGEVA is based on a phenolic structure and could replace DGEBA, the diepoxy found in more than 90% of commercial epoxy formulas and derived from bisphenol A, a known endocrine disruptor.[36]

Polyfunctional epoxy resins can also be obtained from vegetable oils, by oxydation of unsaturated triglycerides (triesters of fatty acid with glycerol, Scheme 2).[36] Epoxidized linseed oil (ELO) was used in this study to cover a broad spectrum of mechanical properties for the final materials.

Finally, a commercial cardanol-based difunctional epoxy (Cardolite NC-514) was also used. Cardanol is extracted from cashew nut shell liquid (CNSL), a waste from the production of cashew nuts. Cardanol is composed of a phenol with a C15 aliphatic side chain (Scheme 3).[38–40] Cardanol can be modified to produce an epoxy resin with an average functionality of 2.[41] These three monomers were endowed with different types of epoxy function, internal, terminal and glycidyl, and thus with different reactivities, which were evaluated with model compounds.

Reactivity study

The reactivity of phosphoric acid towards epoxy moieties was investigated by ^{1}H NMR spectroscopy. Three model molecules were chosen to compare the reactivity of terminal or internal epoxides and of phenolic glycidyl ethers. The monophosphoric acid dibutyl phosphate was chosen to simplify the interpretation of the spectra, and was used in a 10-fold molar excess compared to epoxy groups to conduct the kinetics experiments under pseudo-first order conditions. 9,10-Epoxyoctadecane, 1,2-epoxydodecane and phenyl glycidyl ether were used as epoxy substrates and the disappearance of cyclic ether signals were monitored (Fig. 1).

A 90% conversion was reached in 5 h 50 min for the glycidyl ether, 4 h for the internal epoxide (9,10-epoxyoctadecane) and

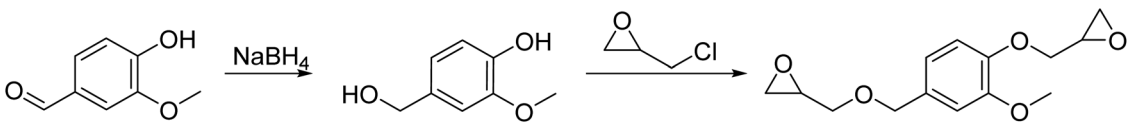

Scheme 1 Synthesis of DGEVA from vanillin.

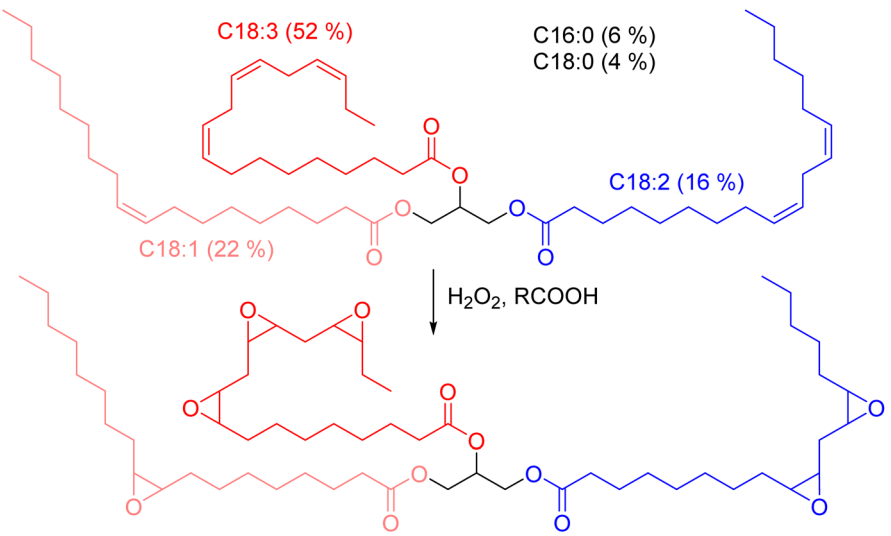

Scheme 2 Epoxidation of vegetable oils unsaturations. Example of the typical triglyceride composition of linseed oil.[37]

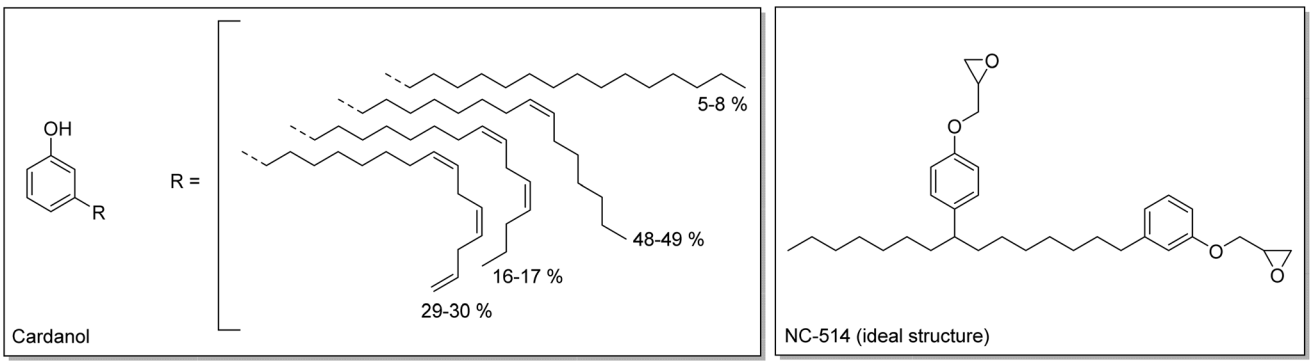

Scheme 3 Structures of cardanol[42] and of NC-514 (ideal structure expected).

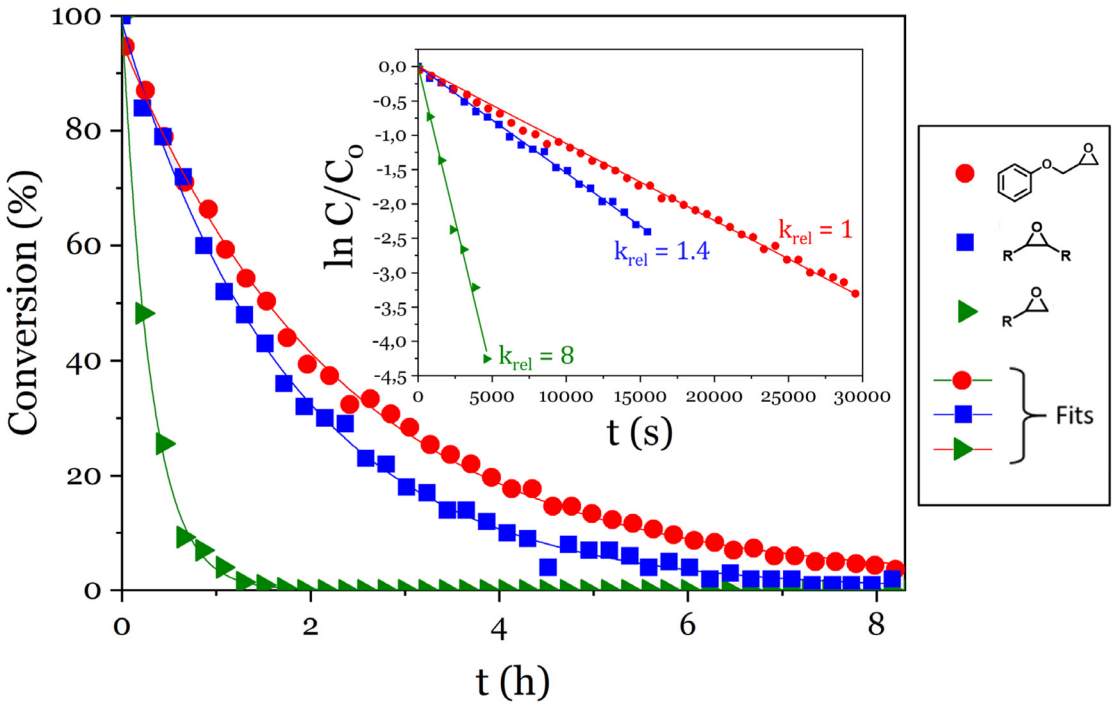

Fig. 1 Evolution of the conversion of the epoxy model molecules *versus* time and pseudo-first order plots (inset).

only 40 min for the terminal epoxide (1,2-epoxydodecane). For each epoxy, $\ln(C/C_0)$ was plotted against time and k_{obs} were determined as the slopes of the linear fits (Fig. 1 inset). The k_{obs} measured this way were $1.120 \pm 0.006\ 10^{-4}\ s^{-1}$, $1.55 \pm 0.01\ 10^{-4}\ s^{-1}$ and $9.0 \pm 0.3\ 10^{-4}\ s^{-1}$ for the glycidyl ether, the internal epoxide and the terminal epoxide, respectively (Fig. 1 inset).

The aliphatic terminal epoxides were converted 8 times faster than the glycidyl ether. Such a difference in reaction rates between the opening of the phenoxyepoxide and of the alkoxyepoxide was unexpected. One possible explanation may be that the phenoxy substituent, slightly less electron donor than its alkoxy counterpart, provides a lower stabilization of the positive charge on the protonated epoxide intermediate. The slight difference in regioselectivity (Scheme 4) is in agreement with this explanation since the phenoxyepoxide led to a greater proportion of terminal phosphate than its alkoxy analog, likely due to the lower stabilization of the secondary (internal) phenoxyepoxide–derived carbocation. However, this explanation remains speculative and was not fully demonstrated. The ring opening reaction was also much faster for terminal epoxy than for internal epoxy, probably due to steric effects.

Although the methodology adopted reveals the consumption of the epoxide functions in presence of phosphoric acid, it does not give access to information about the reactions at stakes and the products formed. Considering the reactions were carried out at room temperature and with a large excess of acid (10 : 1 POH/epoxy), the self-condensation or homopolymerization of epoxides to produce ether bonds is very unlikely.

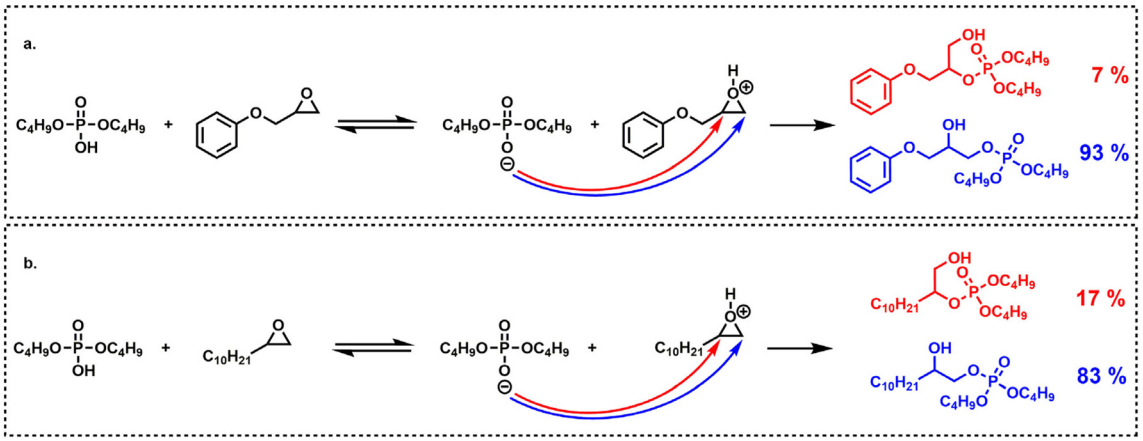

Scheme 4 Regioselectivity (mol%) of oxirane opening by dibutylphosphoric acid on: (a) phenylglycidyl ether and, (b) 1,2-epoxydodecane.

Once the reactivity of the different types of epoxy towards a monophosphoric acid group was verified, reversely the reactivity of the three acid functions of H_3PO_4 towards an epoxy function was also assessed, to ensure the formation of a trisubstituted phosphate ester by this reaction. Thus, the evolution of a binary mixture of 1 equivalent of phosphoric acid and 28 equivalents of phenyl glycidyl ether in acetone was monitored by ^{31}P NMR spectroscopy (≈10 : 1 epoxy/acid functions). In this case, the epoxy order was degenerate and the reactions were run under pseudo-first order for the phosphoric acid. The kinetic equations to model this system are given in ESI.†

The ^{31}P NMR spectra showed that the substitution of the three acid functions happened simultaneously (Fig. 2 and S15–S17†). To simplify the fitting, T was determined as $T = 1 - (A + M + D)$, thus only A, M and D were fitted altogether with the model equations (eqn (S5)–(S8)†), and the values obtained for k_1, k_2 and k_3 were reported in Table 1.

Table 1 Kinetics parameters derived from the fit of the plots shown in Fig. 2

k_1 (h^{-1})	k_2 (h^{-1})	k_3 (h^{-1})	R^2
0.56 ± 0.01	0.62 ± 0.02	1.01 ± 0.03	0.98373

N.B.: the kinetics parameters were determined by a single fit to optimize the three curves at a time.

According to these rate constants values (k_i, i = 1–3), the disubstituted product is more reactive than the monosubstituted product, itself slightly more reactive than the phosphoric acid toward the addition to an epoxy. This result proves that the formation of trisubstituted phosphate esters by reaction of epoxy and phosphoric acid is favored, and could lead to crosslinked networks.

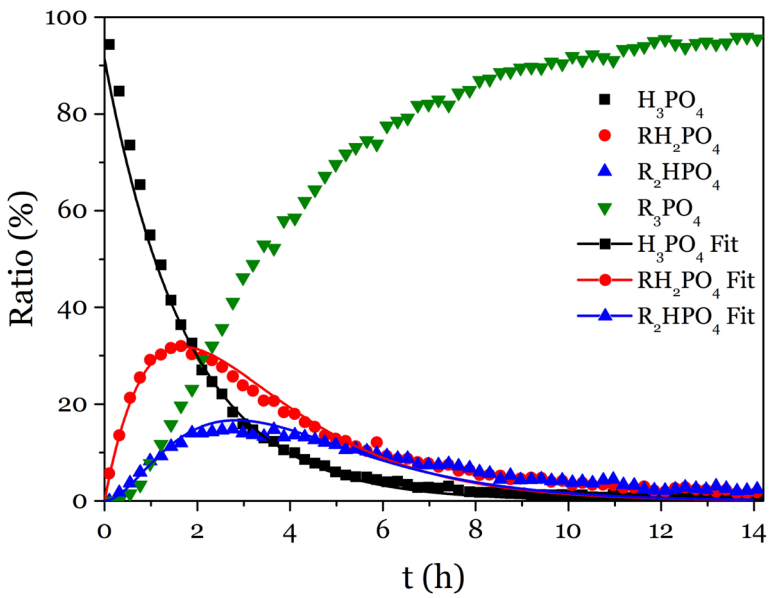

Fig. 2 Evolution with time of the proportion of P-containing species during the reaction of phosphoric acid with phenyl glycidyl epoxy.

Vitrimers synthesis

Vitrimers were synthesized from commercially available bio-based epoxy resins and phosphoric acid using a 1 : 1 epoxy : acid equivalent ratio. The ring opening polymerization of polyfunctional epoxy by phosphoric acid leads to β-hydroxy phosphate esters. Phosphoric acid is trifunctional, it thus played the roles of both hardener and crosslinker (Scheme 5).

DGEVA, ELO and NC-514 were used as epoxy precursors, and the influence of their structures on the materials properties was assessed. The aromatic structure of DGEVA was expected to confer rigidity and thermal resistance to the materials. The aliphatic structure of ELO was expected to lower the T_g and confer flexibility to the final materials. NC-514 was expected to yield materials with intermediate properties compared to DGEVA-based and ELO-based materials.

Due to the strong acidity (pK_a) of phosphoric acid, the reaction with the epoxy ring is fast and very exothermic. The high viscosities of the epoxy resins do not allow an efficient heat dissipation, and the direct mixing of concentrated phosphoric acid and epoxy resin on a 10-grams scale can lead to a thermal runaway. Such runaway reaction effectively happened in the course of this study and led to a small fire which caused limited damage to a lab instrument. To prevent this issue, a solution is to dilute the reaction medium by using a solvent with a suitable boiling point, sufficiently high not to evaporate during the polymerization, but not too high to prevent removal under reduced pressure after synthesis. ELO and DGEVA epoxy resins were thus first diluted with 50 wt% and 20 wt% of acetone, respectively. The formulation for NC-514 was solvent-free owing to the lower reactivity of the glycidyl ether moieties towards phosphoric acid. Then, phosphoric acid was added as a concentrated aqueous solution (Table S1†). After one night at room temperature, the DGEVA, ELO and NC-514 formulations led to a rigid clear yellow material (DGEVAPE, Fig. 3a), a flexible brown material (ELOPE, Fig. 3b) and a flexible dark brown material (CEPE, Fig. 3c), respectively.

Curing

The materials were dried 15 h in an oven at 60 °C and grinded into powders. The powders underwent a curing step at 130 °C under vacuum to ensure complete drying and curing. The dry powders were then pressed at 150 °C for 1.5 h to obtain the final materials.

FTIR revealed that the oxirane C–O–C stretching band at 915 cm^{-1} for NC-514, 918 cm^{-1} for DGEVA (glycidyl ethers) and at 830 cm^{-1} for ELO (aliphatic oxirane) were not visible on the final materials, suggesting that all the epoxy function had reacted (Fig. S1–S3†).

No residual exothermic phenomenon was visible on DSC thermograms and the T_g of the materials were stable at 115 °C, 12 °C and 25 °C for DGEVAPE, ELOPE and CEPE, respectively (Table 2 and Fig. S4–S6†). Thus, the materials were considered fully cured. As expected, DGEVAPE exhibited a high T_g due to the rigidity and high aromatic carbon content of DGEVA and the high crosslinking density, whereas ELOPE had a relatively low T_g due to the flexibility of the fatty chains of ELO. NC-514 which contains both aromatic cycles and aliphatic chains afforded a material (CEPE) with an intermediate T_g. The materials thus prepared cover a large range of T_g and may be suitable to various applications.

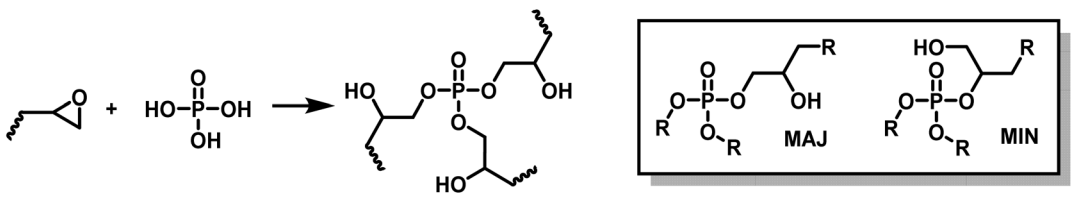

Scheme 5 Synthesis of phosphate triesters by ring opening polymerization (ROP) of epoxides by phosphoric acid.

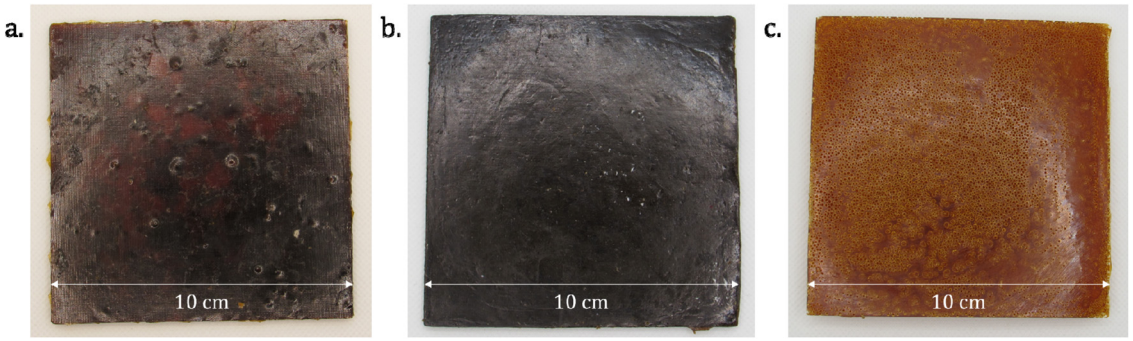

Fig. 3 Photos of (a) DGEVAPE, (b) ELOPE and (c) CEPE.

Table 2 Physicochemical main properties of Vm–RvOH

Material	Epoxy EEW (g eq.$^{-1}$)	T_g (°C)	T_α[a] (°C)	Max tan δ (°C)	E'_G[b] (GPa)	E'_R[c] (MPa)	Gel content[d] (%)	Swelling index[d] (%)
DGEVAPE	269	115	83	121	4.4	6.5	97 ± 2	76 ± 2
ELOPE	191	20	39	60	1.2	1.2	89 ± 1	186 ± 10
CEPE	448	25	22	41	1.6	1.9	71 ± 1	219 ± 14

[a] Determined as the maximum of E''. [b] At −50 °C. [c] At 175 °C. [d] In THF.

The gel contents of the materials were determined in THF. DGEVAPE, ELOPE and CEPE exhibited gel contents values of 97, 89, and 71%, respectively (Table 2). These results confirmed that these materials were indeed crosslinked 3D networks. The swelling indices were 76, 186, and 219% for DGEVAPE, ELOPE and CEPE respectively.

Mechanical characterizations

The thermomechanical properties of the materials were determined by DMA (Table 2 and Fig. S7–S9†). The T_α was determined as the maximum of E'', at 83, 39 and 22 °C for DGEVAPE, ELOPE and CEPE, respectively. Two subvitreous modes (β and γ mechanical relaxations) are visible below T_α for DGEVAPE. A deconvolution of the E'' curve was performed with a sum of three Gaussian curves to determine T_α. The value for DGEVAPE is far from the T_g determined by DSC. This is likely due to the breadth of the transition from the glassy to the rubbery states (Fig. S7†). Similarly, the relatively broad transition for ELOPE can explain the difference between T_g and T_α. For CEPE, the values of T_g and T_α are consistent with each other. Taking into account the broad transition observed for DGEVAPE, the storage modulus values on the glassy plateau and rubbery plateau were taken at −50 °C and +175 °C, respectively, to compare the three materials. The moduli on the glassy plateaus were 4.4, 1.2 and 1.6 GPa for DGEVAPE, ELOPE and CEPE, respectively. This trend was expected as it follows the aromatic carbon content. The moduli on the rubbery plateaus were 6.6, 1.2 and 1.9 MPa, respectively. For a similar matrix, the value of the modulus on the rubbery plateau evolves with the crosslinking density. Here, the polymers have very different structures, thus the values are a combination of these factors and no clear trend can be observed.

The materials are networks of β-hydroxy phosphate triesters. Hydroxyl groups can engage into transesterification with the phosphate esters inducing exchanges in the network. This exchange happens upon heating and leads to the reshaping capability of the materials (Fig. 4). Stress relaxation experiments were performed to characterize the dynamic behavior of the materials. The 3 materials DGEVAPE, ELOPE and CEPE fully relaxed the stress applied above their T_g (Fig. 5). The stress-relaxation curves obtained at different temperatures were fitted with a Kohlrausch–Williams–Watts equation. The relaxation times at 130 °C were 894, 242, and 238 s for DGEVAPE, ELOPE and CEPE, respectively. The long relaxation time of DGEVAPE is not surprising as the transition to the rubbery state for this material was very broad, and extended up to 170 °C. Thus, at 130 °C the stress relaxation is hindered by the alpha relaxation mobility. The relaxation times τ_{KWW} obtained were plotted in an Arrhenius diagram and the flow activation energies, E_a, were calculated from the slope for each material (Table S2†).

These E_a values were 77, 67, and 104 kJ mol^{-1} for DGEVAPE, ELOPE and CEPE respectively. Activation energies depend on the exchange reaction,[5] which is the same in the materials reported here, on the polymer matrix[43] and on the mobility at the local scale.[44–46] The network of CEPE is looser due to the high EEW, so one would expect the activation energy to be lower.[47] The high activation energy might thus be due to the relatively low density of exchangeable bond compared to the other networks presented here.[47] The dangling fatty chains might also play a role as a plasticizer[48] and keep the exchangeable bonds apart. This hypothesis could also explain the slight difference between the activation energies of DGEVAPE and ELOPE.

Thermal and flame retardant properties

Phosphorus-free counterpart materials of DGEVAPE, ELOPE and CEPE, (called DGEVACE, ELOCE and CECE, respectively) but based on citric acid were prepared and examined to highlight the influence of phosphorus in terms of flame retardant (FR) properties. Citric acid was chosen because it is a short trifunctional carboxylic acid, and should thus lead to crosslinking density relatively close to that imparted by phosphoric acid (Table S1†). The thermal properties of the materials were

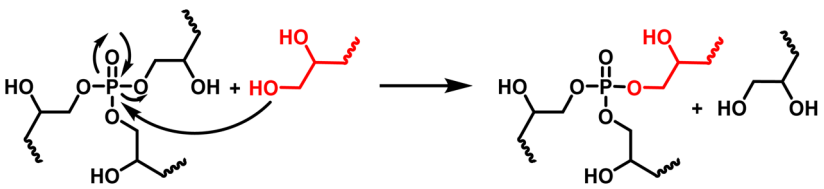

Fig. 4 Exchange in the polymer network by phosphate transesterification.

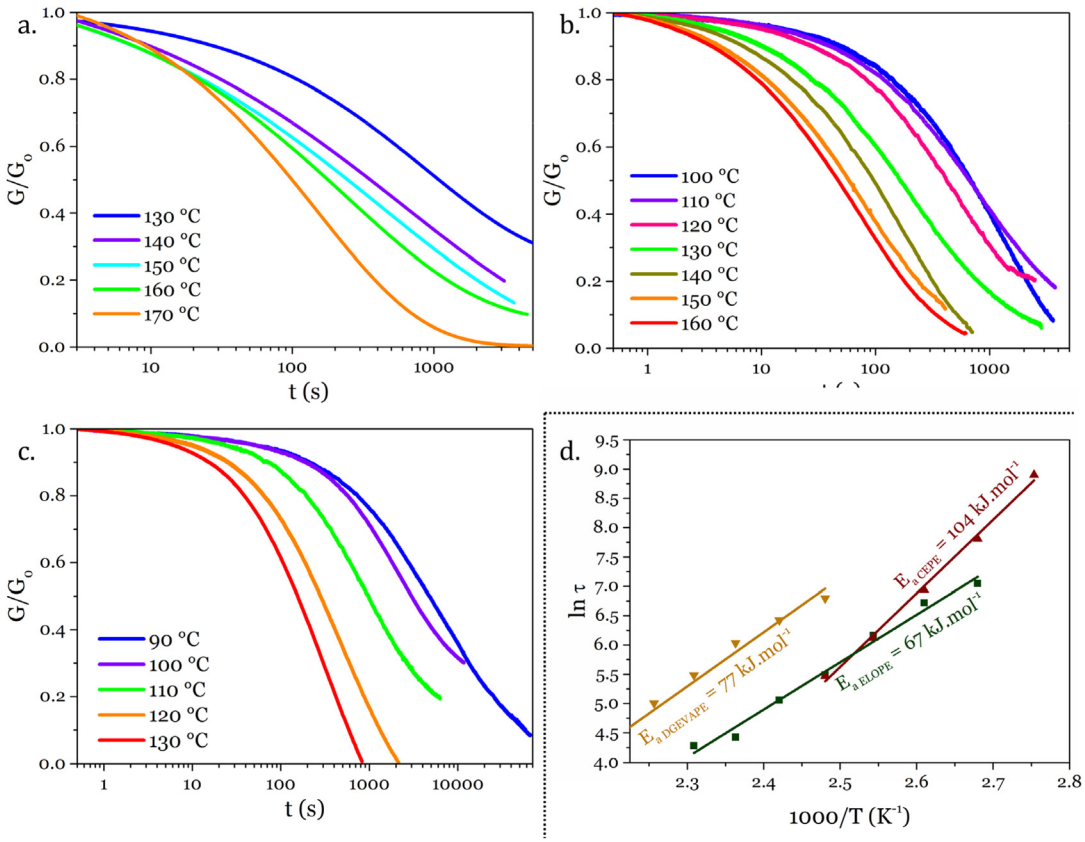

Fig. 5 Stress-relaxation experiments results on (a) DGEVAPE, (b) ELOPE and (c) CEPE. (d) Arrhenius diagram of the τ determined from Kohlrausch–Williams–Watt fits for each material, and determination of the flow activation energies.

first assessed by TGA under nitrogen (Table 3 and Fig. S13†). The temperatures at 5% weight loss were measured at 234, 219, and 298 °C for DGEVAPE, ELOPE and CEPE, and 277, 239 and 305 °C for DGEVACE, ELOCE and CECE, respectively. A single step of decomposition was observed for phosphorus-free counterpart materials and for DGEVAPE contrary to CEPE and ELOPE materials. The temperatures at the maxima of the TG derivatives ($T_{d\ max}$) were 403, 413 and 452 °C for DGEVACE, ELOCE and CECE. DGEVAPE exhibited a single $T_{d\ max}$ at 317 °C, while for ELOPE and CEPE two maxima were visible at 280 and 454 °C, and at 351 and 483 °C, respectively. The decrease of $T_{d5\%}$ for the phosphorus-containing materials compared to phosphorus-free ones is due to the lower stability of the O=P–O bond compared to C–C bond. The phosphate groups first decomposed and during this step, they increased the crosslinking carbonization that prevented further decomposition of the epoxy resin. For CEPE and ELOPE, the second degradation step is the aliphatic chain decomposition (Fig. S13†).[49] Thus, the residues at 700 °C represented 49 wt% for DGEVAPE, 26 and 23 wt% for ELOPE and CEPE, when for DGEVACE, ELOCE and CECE the residues were 16, 2 and 3 wt%, respectively. The first difference of residue yields between the two families (phosphorus-containing and -free materials) is explained by the phosphorus action. The second main difference in residues between aliphatic and aromatic compounds is explained by the interaction of phosphorus and aromatic groups, resulting in polyaromatic char.[50] The better residue yield for ELOPE compared to CEPE is the result of the high phosphorus ratio in this material (9.2 wt% *vs.* 4.3 wt%). Such increase of the residue on phosphorus-containing materials clearly points out its FR efficiency in condensed phase, and the high performance of both materials made with DGEVA is likely due to their high aromatic carbon content, and the high cross-linking density.[51] Indeed, the aromatic

Table 3 Main thermal properties of Vm–RvOH

Material	P ratio[a] (wt%)	$T_{d\ 5\%}$ [b] (°C)	$T_{d\ max}$ [b] (°C)	Residue (char)[b,c] (wt%)
DGEVACE	0	277	403	16
DGEVAPE	6.8	234	317	49
ELOCE	0	239	413	2
ELOPE	9.2	219	280 and 454	26
CECE	0	305	452	3
CEPE	4.3	298	351 and 483	23

[a] Determined as: $P\,\text{ratio(wt\%)} = \frac{\text{number of } P \times M(P)}{\sum_i \text{number of atoms of } i \times M(i)}$, i = element [b] Under nitrogen atmosphere – T_{max}^{d} read on the TG derivatives. [c] At 700 °C.

Table 4 PCFC results of the phosphate ester vitrimers DGEVAPE, ELOPE, CEPE and their carboxylic ester counterparts DGEVACE, ELOCE and CECE

Samples	pHRR (W g^{-1})	T at pHRR (°C)	THR (kJ g^{-1})	Residue content (wt%)	EHC (kJ g^{-1})
DGEVACE	364.3 ± 2	397 ± 3	16.6 ± 0.2	9.1 ± 0.6	18.3 ± 0.2
DGEVAPE	107.9 ± 5	317 ± 1	4.4 ± 0.2	49.4 ± 3	8.7 ± 0.2
ELOCE	268.3 ± 10	407 ± 8	23.5 ± 0.7	1.4 ± 0.6	23.8 ± 0.6
ELOPE	125.2 ± 9	282 ± 2	18.5 ± 0.3	20.6 ± 3	23.3 ± 0.5
	114.5 ± 8	445 ± 3			
CECE	331.3 ± 7	451 ± 6	28.2 ± 0.8	0.0 ± 0.5	28.2 ± 0.8
CEPE	109.3 ± 10	346 ± 5	24.8 ± 1	12.5 ± 3	28.3 ± 0.2
	209.6 ± 10	479 ± 5			

content in CECE is not sufficient to favor the char formation, as the crosslinking density is lower than in DGEVACE.

Flame retardancy were investigated to evaluate the effect of the phosphate esters crosslinking nodes on this property. Table 4 summarizes the data obtained from PCFC analyses and the heat release rate (HRR) *vs.* temperature curves are presented in Fig. 6.

The curves (Fig. 6) showed a strong influence of the phosphate on the FR properties. The peak of heat release rate (pHRR), the total heat release (THR), the energy of combustion (EHC) as well as the residue are important parameters to determine the ability of a material to provide flame retardant properties. First, a fuel release at lower temperature was observed for phosphorus-containing materials compared to phosphorus-free ones. It comes from the early stage of decomposition for phosphorus groups which leads to fuel emission at lower temperature. This decomposition released phosphoric species resulting in high level of charring. The pHRR of the DGEVAPE material was 107.9 W g^{-1}, 70% lower than DGEVACE (364.3 W g^{-1}), with a decrease of the associated temperature, highlighting the early decomposition of phosphate species and the charring effect. Moreover, the ELOPE and the CEPE materials exhibited two pHRR. Those results were consistent with the TGA analysis: one or two peaks were observed corresponding to the decomposition steps. Moreover, the first pHRR could be attributed to the phosphoric acid parts decomposition. That is why the first peak of ELOPE exhibited a value of 125.2 W g^{-1} (slightly higher value due to the phosphorus ratio in the material) and the first peak of CEPE showed a value of 109.3 W g^{-1} which was in the same range as the DGEVAPE

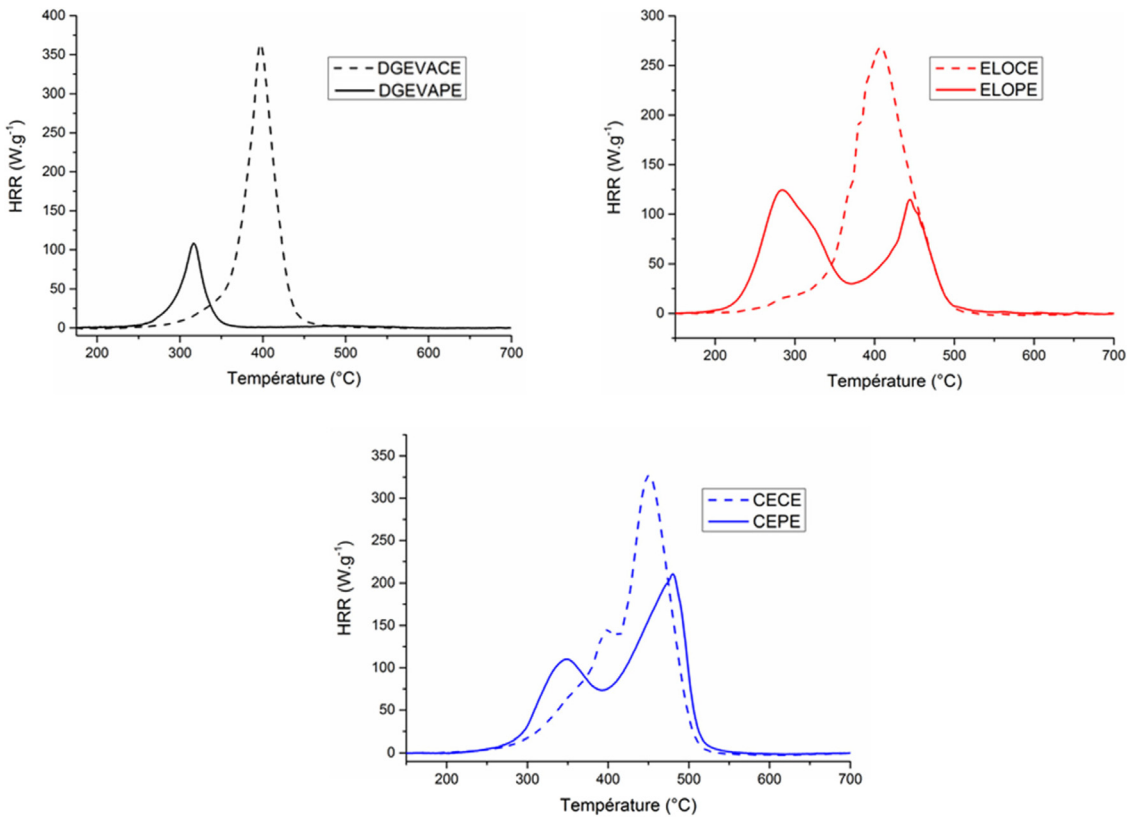

Fig. 6 PCFC curves of the phosphate ester vitrimers DGEVAPE, ELOPE, CEPE and their carboxylic ester counterparts DGEVACE, ELOCE and CECE.

peak. Then, the second pHRR could be mainly ascribed to the decomposition of the aliphatic chains of the network not able to create efficient charring. The effective heat of combustion (EHC) values such as the total heat release (THR) decreased when phosphoric acid was used as crosslinker for the material. The best result was obtained with DGEVAPE because of the absence of aliphatic chains. In fact, these chains are unfavorable to char promotion and contain a high amount of carbon, contributing to heat release. Additionally, the residue contents were consistent with the char content measured by TGA.

Cone calorimetry (Fig. 7) provides important information on the fire behavior of a material.[52] The results of cone calorimeter tests are summarized in Table 5 and Fig. 8 exhibits the associated curves. Time to ignition (TTI) measures the time to achieve sustained flaming combustion at a particular external heat flux. All the TTI were higher for the phosphorus-contain-

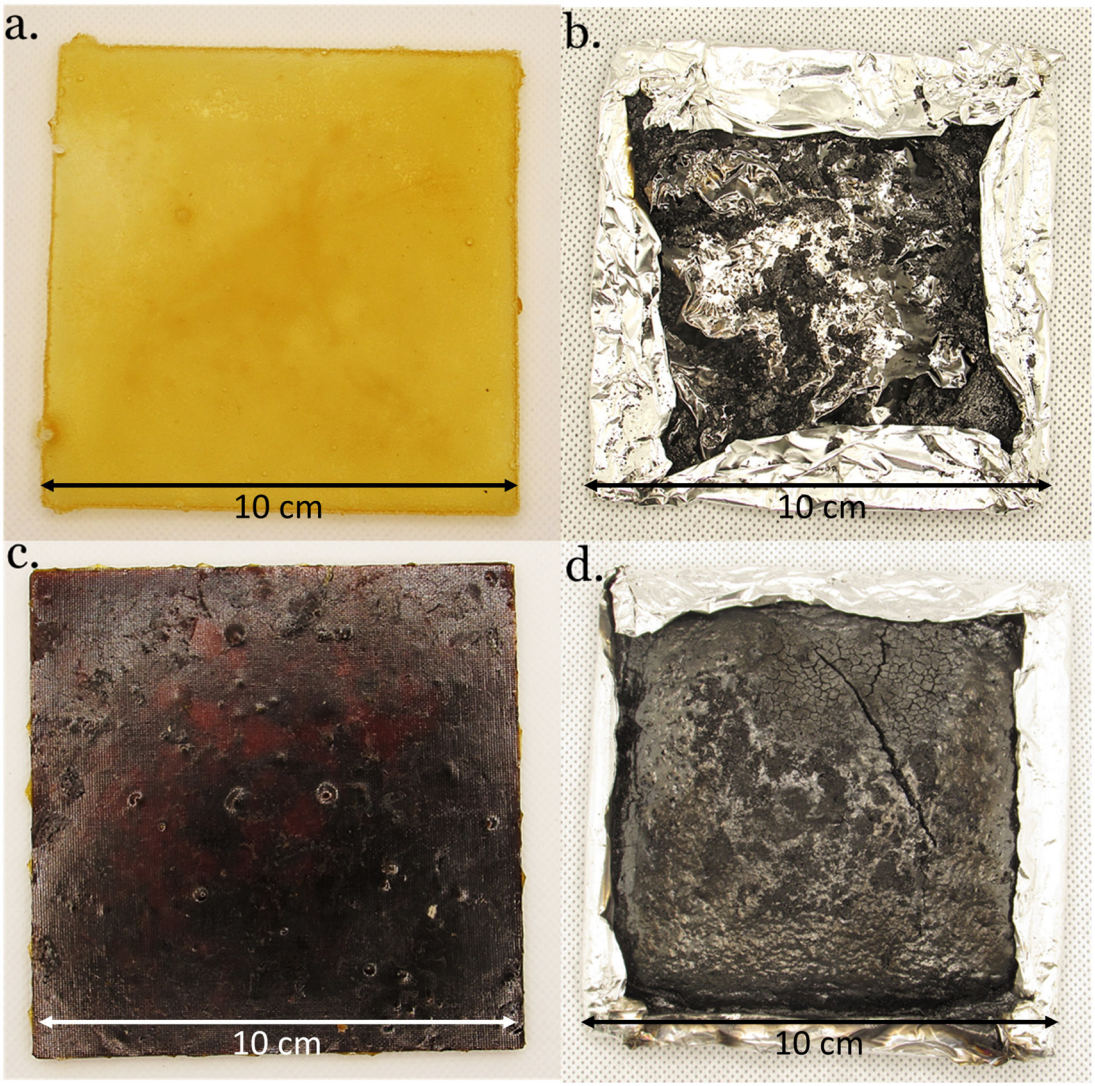

Fig. 7 DGEVACE (reference) (a) before and (b) after cone calorimeter analysis, and DGEVAPE (vitrimer) (c) before and (d) after cone calorimeter analysis.

Table 5 Cone calorimeter results

Samples	TTI (s)	pHRR (kW m^{-2})	THR (MJ g^{-1})	Residue content (wt%)	EHC (MJ kg^{-1})
DGEVACE	77 ± 3	550 ± 9	18.2 ± 0.4	2.6 ± 0.3	18.7 ± 0.4
DGEVAPE	117 ± 4	503 ± 9	6.8 ± 0.2	44.0 ± 0.9	12.1 ± 0.2
ELOCE	19 ± 3	955 ± 10	23.6 ± 0.3	0.4 ± 0.2	23.7 ± 0.3
ELOPE	36 ± 3	907 ± 10	17.3 ± 0.3	21.8 ± 0.5	22.1 ± 0.4
CECE	31 ± 3	1090 ± 12	15.5 ± 0.2	0.1 ± 0.1	15.5 ± 0.2
CEPE	49 ± 4	477 ± 9	7.7 ± 0.4	22.6 ± 0.6	9.9 ± 0.5

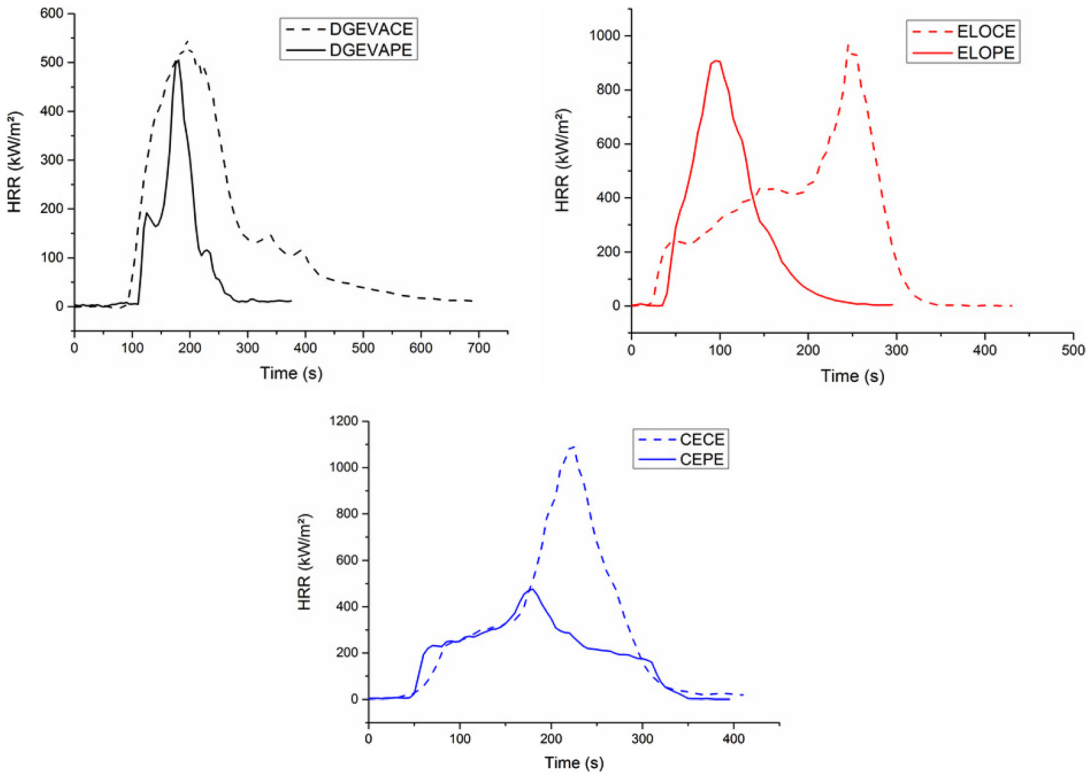

Fig. 8 Cone calorimeter curves of the phosphate ester vitrimers DGEVAPE, ELOPE, CEPE and their carboxylic ester counterparts DGEVACE, ELOCE, CECE.

ing materials. Indeed, DGEVACE exhibited a TTI of 77 s whereas DGEVAPE showed a 44% longer TTI of 117 s. Moreover, the TTI of ELOPE and CEPE were 43% and 37% longer than those of ELOCE and CECE, respectively. Despite a lower degradation temperature measured in TGA, phosphate materials exhibit a higher TTI. This may be ascribed to the lower heat of combustion (EHC) of gases released by the decomposition. Indeed, ignition occurs when a critical density of energy is reached, and this density depends not only on the gases concentration but also on their heat of combustion.[53] The rate of heat release (HRR) and the total heat release (THR) are important parameters to characterize the fire performance of materials. The introduction of phosphoric acid, a phosphate compound, has a strong influence on the THR due to its ability to act in condensed phase. Indeed, the THR of DGEVAPE, ELOPE and CEPE were 63%, 27% and 50% lower than those of DGEVACE, ELOCE and CECE, respectively. From these differences, it is clear that both phosphorus and aromatics are active in improving properties.

The effective heat of combustion (EHC) was also lower for the phosphoric acid-based CANs compared to the citric acid analogs. As expected, the residue contents were higher for the phosphoric acid-containing materials than for the citric acid ones (Fig. 7). This is particularly remarkable in the case of DGEVAPE which residue content reached 44% whereas it was only 2.6% for DGEVACE. The residue content values were consistent with the ones measured by TGA. The decomposition of phosphorus species takes place in the first stage of degradation with the generation of radicals able to initiate effective char entailed insulating effect. Indeed, phosphate functions are known to provide a continuous protective carbon layer due to rearrangement and Diels–Alder reactions.[54] This carbon layer prevent heat and gas transfer between the gas and condensed phases.[55,56]

The pHRR of DGEVAPE and ELOPE was close respectively to their carboxylic ester counterparts DGEVACE and ELOCE. However, the pHRR of CEPE was half lower compared to CECE. An hypothesis which may explain this result relies on the fact that cardanol possesses conjugated double bonds on the alkyl chain, close to an aromatic cycle. In the presence of phosphoric acid, these double bonds favor Diels–Alder reaction responsible for the charring is favored. This charring would protect more efficiently the material against the combustion, which could explain the lower pHRR in the case of cardanol-based materials.

With all the parameters taken into account, the best fire retardancy results were obtained with DGEVAPE and caused by the joint action of the high content of aromatic rings, the high cross-linking ratio, and the presence of phosphate.

Materials from epoxy mixtures

Crosslinked materials prepared from epoxy mixtures were investigated. Four materials were prepared by reacting phosphoric acid with epoxy resin mixtures (Fig. 9, and Table 6).

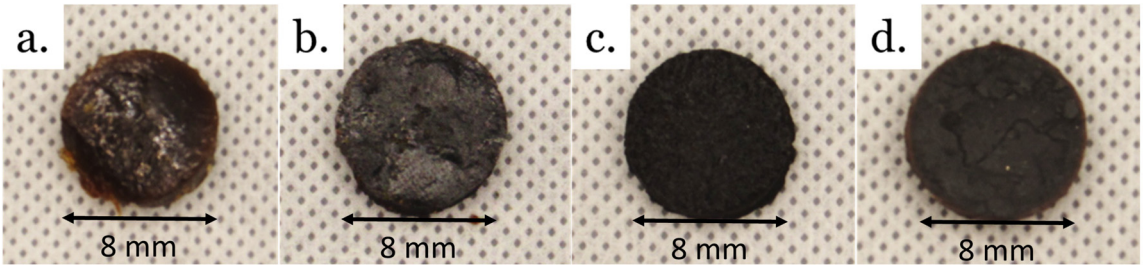

Fig. 9 Pictures of vitrimers from epoxy mixtures. (a) CardELO, (b) CardVAn, (c) VanELO, (d) CardVanELO.

Three materials were prepared from binary mixtures of epoxy: CardVan from NC-514 and DGEVA; VanELO from DGEVA and ELO, and CardELO from NC-514 and ELO. The fourth material, CardVanELO was prepared from an equimolar ternary mixture of NC514, DGEVA and ELO.

All 4 materials exhibited gel contents over 86% (up to 97% for Van ELO), which confirms that crosslinked materials were obtained. The swelling indices of CardVan and VanELO (189% and 85% respectively) were lower than those of CEPE (219%) and ELOPE (186%), confirming that DGEVA densifies the polymer networks.

All materials exhibited a single T_g, indicating homogeneity and the absence of phase segregation (Fig. S14†). The T_g of CardVan is 29 °C, the presence of DGEVA in the formula does not have a significant effect compared to CEPE (T_g = 25 °C). In VanELO this effect is also observed, as DGEVA is the main component, but the T_g remains low at 28 °C, and closer to ELOPE (20 °C). CardELO has a T_g of 38 °C, comparable to the value for CEPE (25 °C), which was expected as NC-514 is the main component and the difference between the T_g of CEPE and ELOPE is low (25 °C and 12 °C). Finally, the T_g of CardVanELO is 24 °C, which can also be expected as 71% of the formula is composed of NC-514 and ELO giving a low T_g compared to DGEVA (Table 7).

TGA under nitrogen of CardVan revealed that the temperature of 5% weight loss at 292 °C is close to the value of CEPE (298 °C) which is the main component, and higher than the value for DGEVAPE (234 °C). VanELO has a higher $T_{d5\%}$ at 262 °C than the two corresponding single-component materials. Interestingly, the residue at 700 °C for CardVan and VanELO are 41 and 44%, close to the value of DGEVAPE (49%) and much higher than the values for CEPE and ELOPE (23% and 26%). Comparatively, the value for CardELO is close to both CEPE and ELOPE, at 23%. As expected, the mixture of DGEVA to other epoxy seems to increase significantly the char

Table 6 Composition of vitrimers from epoxy mixtures

Sample	Mean EEW (g eq.$^{-1}$)	NC-514 (wt%[a])	DGEVA (wt%[a])	ELO (wt%[a])	Acetone (wt%[b])
CardVan	381	62	38	—	0
VanELO	237	—	59	41	50
CardELO	371	70	—	30	20
CardVanELO	340	49	29	22	20

[a] Ratio of the epoxy compared to the total mass of epoxy. [b] Quantity of acetone added relative to the total mass of epoxy.

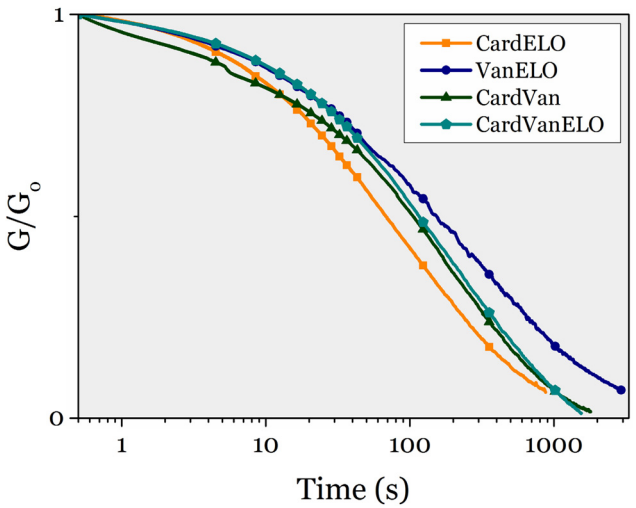

Fig. 10 Stress-relaxation experiments on epoxy mixtures vitrimers at 150 °C.

Table 7 Main properties of vitrimers from epoxy mixtures

Sample	$T_{d\ 5\%}$[a] (°C)	$T_{d\ 50\%}$[a] (°C)	Residue (char)[a,b] (wt%)	Swelling index[c] (%)	Gel content[c] (%)	T_g (°C)
CardVan	292	464	41	189 ± 18	92 ± 2	29
VanELO	262	459	44	85 ± 11	97 ± 1	28
CardELO	282	458	23	204 ± 20	86 ± 2	38
CardVanELO	281	445	31	141 ± 16	88 ± 2	24

[a] Under nitrogen atmosphere. [b] At 700 °C. [c] In THF.

content of the materials obtained. CardVanELO exhibits mean properties between the three monoepoxy materials with a $T_{d5\%}$ of 281 °C and a residue of 31%.

Stress-relaxation experiments were performed at 150 °C on each of these 4 materials. They all relaxed the stress applied, as their three monoepoxy-derived counterparts (Fig. 10).

Conclusion

Biobased vitrimers were synthesized from three biobased epoxy monomers derived from vanillin, linseed oil and cardanol. Phosphoric acid was used as the hardener to prepare networks of trifunctional phosphate esters. The reactivity of phosphoric acid towards epoxy was studied on model molecules by ^{1}H and ^{31}P NMR. The kinetics of the different types of epoxy functions were also compared and showed that internal and terminal aliphatic epoxides are respectively 1.4 and 8 times more reactive compared to glycidyl ether epoxides. The material derived from vanillin exhibited a high T_g due to its high aromatic carbon content, contrary to the aliphatic material made from linseed oil and the material prepared from cardanol containing both aromatic cycles and aliphatic chains. Thanks to the transesterification reaction on phosphate esters and the presence of hydroxy groups in the material, the materials exhibited dynamic properties and could be reprocessed by compression molding without any catalyst. However, ELOPE exhibited a sensitivity to moisture and hydrolysis and flowed after several weeks, which could hinder its use for durable applications. DGEVAPE and CEPE appeared much more resistant to moisture, as they did not flow after over a year without any storage precaution. The high phosphate content, but also a high ratio of aromatic groups for the vanillin-based vitrimer, conferred strong flame retardancy properties to the materials, due to the formation of an insulating char layer during the combustion, limiting the heat flow in the materials. The synthesis of such phosphate vitrimers is straightforward and readily scalable, and the DGEVA could be mixed with ELO and NC-514 to improve the flame retardancy properties, while keeping a relatively low T_g. Such materials could find applications in flexible halogen-free fire-retardant polymers.

Experimental section

Materials

9,10-Epoxyoctadecane (purity not specified), 1,2-epoxydodecane (≥90%) and phenyl glycidyl ether (≥99%) were purchased from Sigma-Aldrich. DGEVA was obtained from Sherwin-Williams (Eposir VANDGE batch RE1086B) and kindly supplied by DIAM Bouchage SAS. Epoxydized cardanol NC-514 was supplied by Cardolite. Epoxydized linseed oil Merginat ELO was supplied by Hobum Oleochemicals GmbH. Phosphoric acid (85% in H_2O), citric acid (99%) and deuterated chloroform (99.8%) were supplied by Sigma-Aldrich. Acetone (≥99.8%) was supplied by Carlo Erba. Deuterated acetone (99.8%) was supplied by Eurisotop.

Synthetic procedures

Mono-epoxy vitrimers. The EEW of the epoxy resins were determined by ^{1}H NMR following the procedure described by Dorsey *et al.*[57] (ESI† part B) DGEVA and ELO were diluted in 20% and 50% of acetone, respectively. Phosphoric acid (85% aqueous) was added to NC-514 or the solutions of DGEVA or ELO at a 1 : 1 epoxy/OH ratio. The mixtures were stirred manually until they were homogeneous (clear) and then were cast in silicone molds. The mixtures were left overnight under a fume hood to slowly evaporate the acetone and allow the polymerization. The materials were then left 16 h at 60 °C under vacuum in an oven, and then 16 h at 130 °C to evaporate acetone and ensure complete polymerization.

Vitrimers from epoxy mixtures. The epoxy resins, and acetone whenever necessary, were mixed in a planetary mixer for 90 s at 3000 rpm. The resulting homogeneous mixtures were then immediately reacted with the adequate amount of phosphoric acid to obtain a 1 : 1 epoxy/OH ratio and the same curing process as the previous materials was applied, one night at 60 °C and one night at 130 °C under vacuum.

Citric acid-crosslinked reference materials. Non-phosphate reference materials (Table S1†) were prepared following the procedure described by Williams *et al.*[58] Citric acid was dissolved in a minimum amount of water at 90 °C. This aqueous solution was mixed with the epoxy at 90 °C for at least 10 min until the initially blurry medium became translucent. The medium was poured in silicone molds and cured 6 h at 90 °C, then overnight at 120 °C.

Instrumentation

NMR. ^{1}H NMR were acquired on a Bruker Avance 400 MHz spectrometer at 23 °C. External reference was tetramethylsilane (TMS) with chemical shifts given in ppm. Samples were diluted in 0.5 mL of $CDCl_3$.

Kinetics study of the epoxy reactivity: 30 to 35 mg of epoxy were dissolved in 0.25 mL of $CDCl_3$. 10 equivalents of dibutyl phosphate were mixed in 0.25 mL of $CDCl_3$. The epoxy and the phosphate solutions were quickly mixed together in a test tube with a vortex, transferred into an NMR tube, which was then placed into the NMR spectrometer as fast as possible, and the NMR data acquisition was started. The disappearance of the peaks associated to the epoxy function was followed with time by ^{1}H NMR.

Kinetics study of the phosphoric acid reactivity: 30 mg of phosphoric acid (85% aqueous solution, 25.5 mg H_3PO_4, 0.26 mmol, 1 eq.) was mixed with 0.25 mL of deuterated acetone. 1 mL of phenyl glycidyl ether (1.109 g, 7.38 mmol, 28 eq.) was mixed with 0.25 mL of deuterated acetone. The two solutions were quickly mixed together in a test tube with a vortex, transferred into an NMR tube, which was then placed into the NMR spectrometer as fast as possible, and the NMR data acquisition was started. The reaction was followed by ^{31}P NMR.

FTIR. FTIR spectra acquired on a ThermoScientific Nicolet iS50 FT-IR equipped with an attenuated total reflectance cell (ATR). The data were analyzed using the software OMNIC Series 8.2 from Thermo Scientific.

Swelling index and gel content. 40 mg of each material was immersed in 10 mL of THF for 24 h with stirring at 200 rpm. The swollen materials were weighed, then dried for 24 h in an oven at 80 °C under vacuum. The dry materials were weighed. The measure was done in triplicates and the values of swelling index and gel content are the average of the 3 measures.

The swelling index (SI) was calculated using eqn (1), where m_2 is the mass of the swollen material and m_1 is the initial mass. The reported SI are average values of three samples.

$$\mathrm{SI} = \frac{m_2 - m_1}{m_1} \times 100 \quad (1)$$

The gel content (GC) was calculated using eqn (2), where m_3 is the mass of the dried material and m_1 is the initial mass. Reported GC are average values of three samples.

$$\mathrm{GC} = \frac{m_3}{m_1} \times 100 \quad (2)$$

Mechanical characterizations. Relaxation experiments were performed on a ThermoScientific Haake Mars 60 rheometer equipped with a Peltier heating cell and using a textured 8 mm plane–plane geometry. A 5 N axial force was applied for DGEVAPE and a 1 N axial force was applied for ELOPE and CEPE. A 1% torsional strain was applied on 8 mm in diameter and 2 mm thick circular samples, and the rubbery modulus evolution with time was monitored.

DMA. Dynamic Mechanical Analyses were carried out on Metravib DMA 25 with Dynatest 6.8 software. Elongational solicitation of samples ($2 \times 3 \times 10$ mm^3) was performed while heating at a rate of 3 °C min^{-1} from −80 °C to 180 °C, keeping the frequency at 1 Hz.

TGA. Thermogravimetric thermograms were recorded on a Netzsch TG 209F1 Libra instrument under a 40 mL min^{-1} nitrogen flux. Approximately 10 mg of sample were used for each analysis. Ramps from 20 to 700 °C were applied at a rate of 20 °C min^{-1}.

DSC. Analyses were carried out using a NETZSCH DSC200F3 calorimeter. The calibration was performed using adamantane, biphenyl, indium, tin, bismuth and zinc standards. Nitrogen was used as purge gas. Approximately 10 mg of sample were placed in perforated aluminum pans and the thermal properties were recorded between −50 °C and $T_{d2\%}$ −10 °C at 20 °C min^{-1}. The reported values are the values measured during the second heating ramp.

Reprocessing. The materials were grinded with a manual stainless steel coffee grinder. The powders were then pressed under a 6 tons load in a PTFE mold for 2 h at 150 °C for DGEVAPE and for 45 minutes at 120 °C for ELOPE and CEPE, using a Carver 3960 manual heating press.

Pyrolysis combustion flow calorimeter analysis

Fire behavior of vitrimers was analyzed using a pyrolysis combustion flow calorimeter (PCFC). About 3–4 mg were placed in the pyrolyzer, undergoing an increase of temperature from 20 °C to 750 °C at a rate of 1 °C s^{-1} under a nitrogen flow. Pyrolytic gases were sent to a combustor heated at 900 °C under air flow (N_2/O_2 = 80/20). At this temperature and with 20% of oxygen, combustion was considered to be complete. HRR was determined according to oxygen depletion (Huggett's relation) as cone calorimeter test. PCFC analyses correspond to anaerobic pyrolysis followed by high temperature oxidation of decomposition products (complete combustion).[59] All samples were tested in triplicate. The EHC (effective heat of combustion) is the heat released in relation to the quantity of volatile products between the TTI and the extinction time, and mathematically represents the total heat released divided by the loss of mass in the same time.

Cone calorimeter test

Flammability was studied using a cone calorimeter in order to investigate the fire behavior of the samples. The samples dimensions were $100 \times 100 \times 3$ mm^3. All the samples exhibited a weight of 45 g ± 2 g. The samples were placed at 2.5 cm below a conic heater and isolated by rock wool. The samples were exposed to a 35 kW m^{-2} heat flux in well-ventilated conditions (air rate 24 L s^{-1}) in the presence of a spark igniter to force the ignition. Heat release rate (HRR) was determined by oxygen depletion according to Huggett principle (1 kg of consumed oxygen corresponds to 13.1 MJ of heat released).[58] Peak of Heat Release Rate (pHRR) is the maximal value of the heat release rate. The total heat released (THR) was obtained by integration of HRR curves. All samples were tested in triplicate.

Conflicts of interest

There are no conflicts of interest to declare.

Acknowledgements

This work was funded by the Institut Carnot Chimie Balard CIRIMAT (16CARN000801) and the French National Research Agency ANR (AFCAN project – ANR-19-CE06-0014). FC would like to thank Professor Rinaldo Poli for his help on the mathematical treatment of the H_3PO_4-epoxy reactivity kinetics study. SC would like to thank Diam Bouchage for the supply of DGEVA. MD and CN would like to thank Dr Rodolphe Sonnier and Loic Dumazert for their help with the cone calorimetry and PCFC analyses.

References

1 W. Denissen, J. M. Winne and F. E. Du Prez, *Chem. Sci.*, 2016, 7, 30–38.

2 J. M. Winne, L. Leibler and F. E. Du Prez, *Polym. Chem.*, 2019, **10**, 6091–6108.
3 D. Montarnal, M. Capelot, F. Tournilhac and L. Leibler, *Science*, 2011, **334**, 965–968.
4 J. Zheng, Z. M. Png, S. H. Ng, G. X. Tham, E. Ye, S. S. Goh, X. J. Loh and Z. Li, *Mater. Today*, 2021, **51**, 586–625.
5 F. Cuminet, S. Caillol, É. Dantras, É. Leclerc and V. Ladmiral, *Macromolecules*, 2021, **54**, 3927–3961.
6 W. Denissen, G. Rivero, R. Nicolaÿ, L. Leibler, J. M. Winne and F. E. Du Prez, *Adv. Funct. Mater.*, 2015, **25**, 2451–2457.
7 X. Liu, L. Liang, M. Lu, X. Song, H. Liu and G. Chen, *Polymer*, 2020, **210**, 123030.
8 Y.-X. X. Lu, F. Tournilhac, L. Leibler and Z. Guan, *J. Am. Chem. Soc.*, 2012, **134**, 8424–8427.
9 O. R. Cromwell, J. Chung and Z. Guan, *J. Am. Chem. Soc.*, 2015, **137**, 6492–6495.
10 Y. Nishimura, J. Chung, H. Muradyan and Z. Guan, *J. Am. Chem. Soc.*, 2017, **139**, 14881–14884.
11 F. Cuminet, D. Berne, S. Lemouzy, E. Dantras, C. Joly-Duhamel, S. Caillol, E. Leclerc and V. Ladmiral, *Polym. Chem.*, 2022, **8**, 5255–5446.
12 D. Berne, F. Cuminet, S. Lemouzy, C. Joly-Duhamel, R. Poli, S. Caillol, E. Leclerc and V. Ladmiral, *Macromolecules*, 2022, **55**, 1669–1679.
13 M. Delahaye, J. M. Winne and F. E. Du Prez, *J. Am. Chem. Soc.*, 2019, **141**, 15277–15287.
14 H. Zhang, S. Majumdar, R. A. T. M. van Benthem, R. P. Sijbesma and J. P. A. Heuts, *ACS Macro Lett.*, 2020, **9**, 272–277.
15 S. Penczek, J. B. Pretula, K. Kaluzynski and G. Lapienis, *Isr. J. Chem.*, 2012, **52**, 306–319.
16 Z. Zhou, X. Su, J. Liu and R. Liu, *ACS Appl. Polym. Mater.*, 2020, **2**, 5716–5725.
17 E. Rossegger, R. Höller, D. Reisinger, M. Fleisch, J. Strasser, V. Wieser, T. Griesser and S. Schlögl, *Polymer*, 2021, **221**, 123631.
18 K. Moazzen, E. Rossegger, W. Alabiso, U. Shaukat and S. Schlögl, *Macromol. Chem. Phys.*, 2021, **222**, 2100072.
19 F. Chen, Q. Cheng, F. Gao, J. Zhong, L. Shen, C. Lin and Y. Lin, *Eur. Polym. J.*, 2021, **147**, 110304.
20 C. Dertnig, G. Guedes de la Cruz, D. Neshchadin, S. Schlögl and T. Griesser, *Angew. Chem., Int. Ed.*, 2023, **62**, e202215525.
21 M. Bergoglio, D. Reisinger, S. Schlögl, T. Griesser and M. Sangermano, *Polymers*, 2023, **15**, 1024.
22 U. Shaukat, E. Rossegger and S. Schlögl, *Polymer*, 2021, **231**, 124110.
23 L. Cheng, S. Liu and W. Yu, *Polymer*, 2021, **222**, 123662.
24 S. Majumdar, B. Mezari, H. Zhang, J. Van Aart, R. A. T. M. Van Benthem, J. P. A. Heuts and R. P. Sijbesma, *Macromolecules*, 2021, **54**, 7955–7962.
25 J.-H. Lu, Z. Li, J.-H. Chen, S.-L. Li, J.-H. He, S. Gu, B.-W. Liu, L. Chen and Y.-Z. Wang, *Research*, 2022, **2022**, 9846940, DOI: **10.34133/2022/9846940**.
26 X. Feng and G. Li, *Chem. Eng. J.*, 2021, **417**, 129132.
27 X. Feng and G. Li, *ACS Appl. Mater. Interfaces*, 2020, **12**, 57486–57496.
28 R. Wink, S. Majumdar, R. A. T. M. van Benthem, J. P. A. Heuts and R. P. Sijbesma, *Polym. Chem.*, 2023, **14**, 4294–4302.
29 Y. Chen, Y. Zeng, Y. Wu, T. Chen, R. Qiu and W. Liu, *ACS Appl. Mater. Interfaces*, 2023, **15**, 5963–5973.
30 L. Huang, Y. Yang, Z. Niu, R. Wu, W. Fan, Q. Dai, J. He and C. Bai, *Macromol. Rapid Commun.*, 2021, **42**, 2100432.
31 Y. Liu, B. Wang, S. Ma, X. Xu, J. Qiu, Q. Li, S. Wang, N. Lu, J. Ye and J. Zhu, *Eur. Polym. J.*, 2021, **144**, 110236.
32 S. Majumdar, H. Zhang, M. Soleimani, R. A. T. M. van Benthem, J. P. A. Heuts and R. P. Sijbesma, *ACS Macro Lett.*, 2020, **9**, 1753–1758.
33 M. Fache, E. Darroman, V. Besse, R. Auvergne, S. Caillol and B. Boutevin, *Green Chem.*, 2014, **16**, 1987–1998.
34 E. A. B. da Silva, M. Zabkova, J. D. Araújo, C. A. Cateto, M. F. Barreiro, M. N. Belgacem and A. E. Rodrigues, *Chem. Eng. Res. Des.*, 2009, **87**, 1276–1292.
35 A. Almena and M. Martín, *Ind. Eng. Chem. Res.*, 2016, **55**, 3226–3238.
36 R. Auvergne, S. Caillol, G. David, B. Boutevin and J.-P. Pascault, *Chem. Rev.*, 2014, **114**, 1082–1115.
37 H. B. W. Patterson, *Hydrogenation of Fats and Oils: Theory and Practice*, 2nd edn, 2011, pp. 189–278.
38 M. Ionescu, X. Wan, N. Bilić and Z. S. Petrović, *J. Polym. Environ.*, 2012, **20**, 647–658.
39 W. S. J. Li, F. Cuminet, V. Ladmiral, P. Lacroix-Desmazes, S. Caillol and C. Negrell, *Prog. Org. Coat.*, 2021, **153**, 106093.
40 C. K. S. Pillai, V. S. Prasad, J. D. Sudha, S. C. Bera and A. R. R. Menon, *J. Appl. Polym. Sci.*, 1990, **41**, 2487–2501.
41 F. Jaillet, E. Darroman, B. Boutevin and S. Caillol, *OCL*, 2016, **23**, D511.
42 S. Caillol, *Curr. Opin. Green Sustain. Chem.*, 2018, **14**, 26–32.
43 M. Guerre, C. Taplan, J. M. Winne and F. E. Du Prez, *Chem. Sci.*, 2020, **11**, 4855–4870.
44 F. Meng, M. O. Saed and E. M. Terentjev, *Nat. Commun.*, 2022, **13**, 5753.
45 B. R. Elling and W. R. Dichtel, *ACS Cent. Sci.*, 2020, **14**, 53.
46 A. Breuillac, A. Kassalias and R. Nicolaÿ, *Macromolecules*, 2019, **52**, 7102–7113.
47 Y. Spiesschaert, C. Taplan, L. Stricker, M. Guerre, J. M. Winne and F. E. Du Prez, *Polym. Chem.*, 2020, **11**, 5377–5385.
48 C. Li, S. Zhang and B. Ju, *Ind. Crops Prod.*, 2023, **191**, 115941.
49 Q. Wang and W. Shi, *Polym. Degrad. Stab.*, 2006, **91**, 1289–1294.
50 U. Braun, A. I. Balabanovich, B. Schartel, U. Knoll, J. Artner, M. Ciesielski, M. Döring, R. Perez, J. K. W. Sandler, V. Altstädt, T. Hoffmann and D. Pospiech, *Polymer*, 2006, **47**, 8495–8508.
51 R. Ménard, C. Negrell, M. Fache, L. Ferry, R. Sonnier and G. David, *RSC Adv.*, 2015, **5**, 70856–70867.

52 T. McNally, P. Pötschke, P. Halley, M. Murphy, D. Martin, S. E. J. Bell, G. P. Brennan, D. Bein, P. Lemoine and J. P. Quinn, *Polymer*, 2005, **46**, 8222–8232.
53 R. E. Lyon and J. G. Quintiere, *Combust. Flame*, 2007, **151**, 551–559.
54 J. Green, *J. Fire Sci.*, 1996, **14**, 353–366.
55 J. Qi, Q. Wen and W. Zhu, *IOP Conf. Ser.: Mater. Sci. Eng.*, 2018, **392**, 032007.
56 S. Hamdani, C. Longuet, D. Perrin, J. M. Lopez-Cuesta and F. Ganachaud, *Polym. Degrad. Stab.*, 2009, **94**, 465–495.
57 J. G. Dorsey, G. F. Dorsey, A. C. Rutenberg and L. A. Green, *Anal. Chem.*, 1977, **49**, 1144–1145.
58 F. I. Altuna, V. Pettarin and R. J. J. Williams, *Green Chem.*, 2013, **15**, 3360–3366.
59 C. Huggett, *Fire Mater.*, 1980, **4**, 61–65.